

UV-Assisted Fabrication of Reduced Graphene Oxide Doped $\text{SiO}_2@\text{TiO}_2$ Nanocomposites as Efficient Photocatalyst for Photodegradation of Rhodamine B¹

Xueqin Wang^a, Junlei Wang^a, Zhaoliang Ding^b, Ningfang Zhu^{a,c}, Fang Wang^a, Kai Cheng^a, Qihui Chen^a, and Hua Song^{a,*}

^a College of Chemistry & Chemical Engineering, Northeast Petroleum University,
Daqing 163318, Heilongjiang, China

*e-mail: wangji624@163.com

^b High Pressure Workshop of Plastic Plant, PetroChina Daqing Petrochemical Company,
Daqing 163000, Heilongjiang, China

^c Panzhihua Iron and Steel Research Institute, Panzhihu 617000, Sichuan, China

Received November 30, 2017

Abstract—The core-shell nanostructure materials have gained great interests because of its excellent photocatalytic properties and promising applications in several fields. In this work, we prepared the core-shell $\text{SiO}_2@\text{TiO}_2$ nanocomposites by the versatile kinetics-controlled coating method. The graphene oxide (GO) was further reduced over $\text{SiO}_2@\text{TiO}_2$ using UV-assisted photocatalytic reduction method. The physicochemical properties of the as-prepared $\text{SiO}_2@\text{TiO}_2/\text{RGO}$ nanocomposites were characterized by SEM, XRD, BET, EDS, and FTIR. Results showed that, TiO_2 was mainly composed of anatase phase with high crystallinity. Their photocatalytic activities were examined by the degradation of Rhodamine B (RhB) under UV light irradiation. The presence of RGO obviously improved the adsorption ability and photodegradation performance of the composites to RhB. The degradation kinetics of RhB can be described by the pseudo-first-order model. The optimum mass ratio of $\text{SiO}_2@\text{TiO}_2$ to RGO in the composite was 1/0.05 and the rate constant was about 4 times greater than that of the $\text{SiO}_2@\text{TiO}_2$.

DOI: 10.1134/S1070427218050063

INTRODUCTION

Among the past centuries, many environmental problems caused by the fossil fuels remain threat to the human beings. The fossil fuels are not renewable, abundant and eco-friendly resources.

Therefore, looking for the alternative renewable energy such as solar energy [1], biological energy, wind energy and tidal energy is of crucial issue for the support and development of modern society. Solar energy as an abundant, long lasting and clean energy has been explored in some areas especially the photocatalytic area [2]. Titanium dioxide (TiO_2) is one of the mostly investigated semiconductor materials, which characterized by good chemical and thermal stability, excellent electronic and

optical properties with low cost [3]. It is widely used in photocatalytic applications, such as hydrogen evolution [4], water purification, dye sensitization [5], etc. However, owing to the wide band gap of the TiO_2 (3.2 eV for anatase), it has low photo-conversion efficiency under irradiation of solar light which contains of UV with a fraction of only 5% [6]. Besides, pure TiO_2 materials have relatively small surface area, so that the concentration of reactants adsorbed around the active centers is low, which will also reduce the photocatalytic activity [7, 8].

Novel nanostructure materials could exhibit favorable properties compared to the bulk TiO_2 . The core-shell nanostructure materials own large specific surface area and pore volume, providing number density of redox reaction sites on the catalyst surface [9]. For instance, $\text{Pt}@\text{SiO}_2$, $\text{Au}@\text{SiO}_2$, $\text{Au}@\text{SnO}_2$, $\text{RG-O/Fe}_2\text{O}_3$ have been

¹ The text was submitted by the authors in English.

demonstrated in several system for different applications [10]. The Pt@CoO could act as a catalyst for ethylene hydrogenation, whereas amorphous CoO shells transfer gas-phase reactants and products, which is expected to show interesting catalytic behaviors for gas and solution phase reactions [11]. RGO/Fe₂O₃ exhibit better cycling performance and Li storage properties for lithium storage, which is promoting on the Li ion batteries. The core-shell SiO₂@TiO₂ has been applied to gas sensors, catalysts and electrode materials especially the decomposition of dyes [12, 13]. However, due to the low efficiency use of wide energy window of sunlight for the TiO₂, many efforts have to be invested to enhance the photocatalytic activity.

To efficiently enhance the photocatalytic activity of TiO₂, several strategies have been proposed including the preparation of TiO₂-based composites, the metal ion doping, non-metals and photosensitizer modification. Doping TiO₂ with non-metals has been extensively explored to improve its photo-efficiency and broaden its photoabsorption to the visible region resulting from decreasing the band gap of TiO₂ by substituting lattice oxygen with nonmetal elements such as C, N, and F [14, 15]. Among the non-metals, graphene nanosheets as a new type of two-dimensional carbon nanomaterials, a monolayer of carbon atoms arranged in a honeycomb network, exhibit superior electrical conductivity, excellent mechanical flexibility, large surface area, and high thermal/chemical stabilities[16]. The recombination of photo- or electro-chemically generated electron-hole pairs can be slow, when the graphene is hybridized with other materials, leading to the charge transfer rate of electrons and surface-adsorbed amount of chemical molecules through $\pi-\pi$ interactions [11, 17]. In generally, graphene nanosheets would be interesting to be explored in the photocatalytic area [18, 19].

Here, we report a simple procedure to synthesize core-shell SiO₂@TiO₂ nanoparticles with reduced graphene oxide under visible light irradiation. The core-shell SiO₂@TiO₂ nanoparticles are prepared via the versatile kinetics-controlled coating method. Then, different mass ratio of reduction graphene oxide (RGO) was further deposited over SiO₂@TiO₂ using UV-assisted photocatalytic reduction method and the physicochemical properties were characterized. The effect of mass ratio of RGO on the photocatalytic performance of SiO₂@TiO₂/RGO nanoparticles is investigated by photodegradation of RhB and analysis of the reaction kinetics.

EXPERIMENTAL

Synthesis of core-shell structured SiO₂@TiO₂. The SiO₂ particles (purchased from Shanghai Siyu Tech. Co.) were firstly dispersed in 20 mL ethanol by sonication for 30 min. Next 0.1 g of hydroxypropyl cellulose (HPC, 0.1 g) and 0.1 mL de-ionized water were added. After stirring for another 30 min, the mixture of 1 mL titanium *tert*-butoxide (TBOT) and 5 mL ethanol was injected into the previous SiO₂ suspension using a syringe pump at a rate of 0.5 mL min⁻¹. After injection, the mixture was stirred and refluxed for another 100 min at the temperature of 85°C. The products were collected by centrifugation, and washed with ethanol for several times. Finally, the SiO₂@TiO₂ materials were dried at 100°C and then annealed at 450°C for 2 h.

Preparation of SiO₂@TiO₂/RGO nanocomposites. GO was prepared according to a modified Hummer's method. The 0.2 g annealed SiO₂@TiO₂ nanoparticles were firstly dispersed in 200 mL ethanol by sonication for 30 min. Then different amount of GO suspension (0.2 mg mL⁻¹) was added and the mixture was stirred vigorously for 1 h to obtain a homogeneous suspension. The suspension was kept, agitated under UV irradiation for another 1 h to reduce GO to RGO. The resultant composites were collected by centrifugation, washed repeatedly with water, and dried in vacuum at 333 K. The sample with no RGO doping was named as SiO₂@TiO₂, and others were denoted as SiO₂@TiO₂/RGO(1/x), in which x indicated the mass ratio of doped RGO compared to the mass of SiO₂@TiO₂ composites.

Characterization methods. Powder X-ray diffraction (XRD) patterns were collected on a D/max-2200PC diffractometer with CuK_{α1} radiation (40 kV, 30 mA) for the characterization of crystalline structure of SiO₂@TiO₂/RGO nanocomposites. The micromorphology of the series materials were measured by scanning electron microscopy (SEM) on a NOVA600 microscope operated at an acceleration voltage of 5.0 kV. Transmission FTIR spectra were recorded on a Tensor 27 instrument equipped with a resolution of 4 cm⁻¹.

Photo-reactivity measurement. The photocatalytic reactions were performed in a sealed quartz flask (100 mL) at room temperature and oxygen atmosphere. For each measurement, 20 mg of as-synthesized catalyst was dispersed in 40 mL RhB solution (10 μM) and then stirred for 30 min in dark to attain the adsorption-

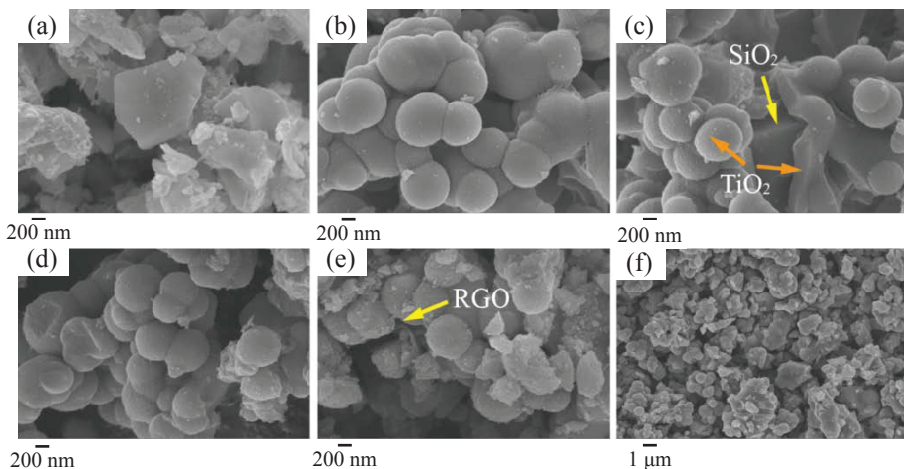


Fig. 1. The SEM images of (a) pure SiO_2 (b and c) $\text{SiO}_2@\text{TiO}_2$ (d) $\text{SiO}_2@\text{TiO}_2/\text{RGO}$ (0.05) (e) $\text{SiO}_2@\text{TiO}_2/\text{RGO}$ (0.2) with the magnification of 50,000 X and (f) $\text{SiO}_2@\text{TiO}_2/\text{RGO}$ (0.05) with the magnification of 10 000 \times .

desorption equilibrium. The photocatalytic reactions were initiated by continuously irradiating the suspension using a 250 W high pressure mercury lamp as light source. An aliquot of 2 mL suspension was collected at given time intervals. The aliquots were immediately centrifuged and analyzed using an UV-vis spectrophotometer (UV-1800, Shimadzu). The concentration of RhB was calculated using the Beer–Lambert Law.

RESULTS AND DISCUSSION

The physicochemical properties of $\text{SiO}_2@\text{TiO}_2/\text{RGO}$ nanocomposites.

The micromorphology of

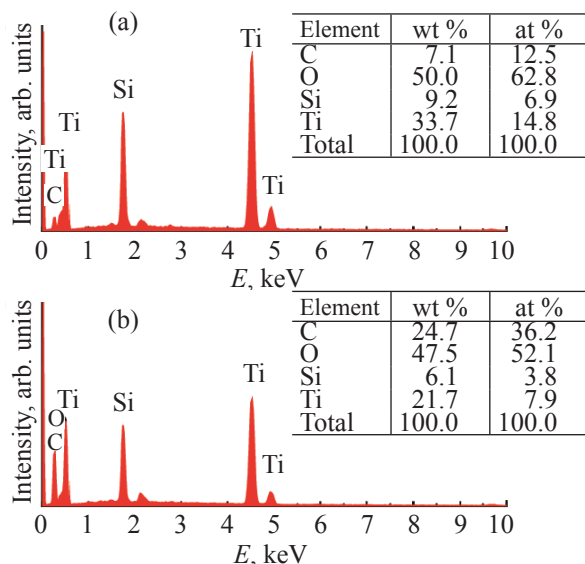


Fig. 2. EDS spectra of (a) the $\text{SiO}_2@\text{TiO}_2$ and (b) the $\text{SiO}_2@\text{TiO}_2/\text{RGO}$ (1/0.05), the according content of each element were inserted in the figures, respectively.

$\text{SiO}_2@\text{TiO}_2$ and $\text{SiO}_2@\text{TiO}_2/\text{RGO}$ nanocomposites was investigated by SEM, as shown in Fig. 1. Figure 1a was SEM image of original SiO_2 core material, which was plate-like shape with smooth surface. After coating with TiO_2 , there was grape-shape nanoparticles originated from SiO_2 surface (Fig. 1b). By investigating the crack area of $\text{SiO}_2@\text{TiO}_2$ nanocomposites (Fig. 1b) we can find that, the thickness of the TiO_2 shell was around 250 nm. After deposition of RGO by UV-irradiation reduction method, the apparent morphology of $\text{SiO}_2@\text{TiO}_2/\text{RGO}$ nanocomposites was barely changed (Fig. 1d, f). When the mass ratio of RGO increased to 0.2, the RGO sheet could be easily found wrapping around the $\text{SiO}_2@\text{TiO}_2$ nanoparticles (Fig. 1e).

Figure 2 shows the EDS spectra of $\text{SiO}_2@\text{TiO}_2$ (Fig. 2a) and $\text{SiO}_2@\text{TiO}_2/\text{RGO}$ (Fig. 2b) nanocomposites. Their components were shown in the insets of Fig. 2a and 2b, respectively. We can find that, the $\text{SiO}_2@\text{TiO}_2$ and $\text{SiO}_2@\text{TiO}_2/\text{RGO}$ were mainly composed of Ti, Si, O, and C elements.

The molar ratio of Ti and Si is around 2.1 : 1, which was similar in both the materials before and after RGO doping. After doping of RGO (Fig. 2b), the composition of C increased from 12.5 to 36.1%, which confirms the successful doping of RGO.

Figure 3 shows the FTIR spectra of $\text{SiO}_2@\text{TiO}_2$ and $\text{SiO}_2@\text{TiO}_2/\text{RGO}$ (1/0.05) nanocomposites. The FTIR spectra of $\text{SiO}_2@\text{TiO}_2$ and $\text{SiO}_2@\text{TiO}_2/\text{RGO}$ showed a similar shape. It can be clearly seen that the peaks located at 3405 cm^{-1} are due to the H–O–H stretching vibration of the free or adsorbed water. The adsorption peak at 1630 cm^{-1} can be attributed to the Ti–O–Ti stretching

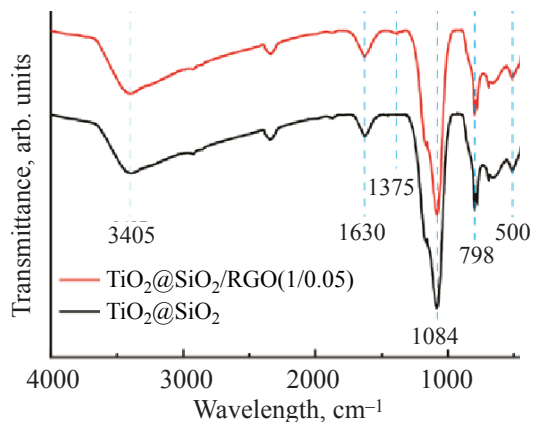


Fig. 3. The FTIR spectra of $\text{SiO}_2@\text{TiO}_2$ and $\text{SiO}_2@\text{TiO}_2/\text{RGO}(1/0.05)$ nanocomposites

vibration or the deformation of water molecules. The peaks centered at 1084 and 798 cm^{-1} are caused by the strong asymmetric stretching and symmetric vibration of $\text{Si}-\text{O}-\text{Si}$, respectively. The broad absorption bands of the stretching and binding modes of $\text{Ti}-\text{O}$ and $\text{Ti}-\text{O}-\text{Ti}$ appears around 500 cm^{-1} . For $\text{SiO}_2@\text{TiO}_2/\text{RGO}$ nanocomposite, a weak adsorption peak appears at about 1375 cm^{-1} which can be attributed to the presence of RGO. The FTIR results further confirm the successful reduction of GO onto $\text{SiO}_2@\text{TiO}_2$ surface by photo-reduction method.

The crystallite structure of $\text{SiO}_2@\text{TiO}_2$ and $\text{SiO}_2@\text{TiO}_2/\text{RGO}$ nanocomposites were characterized by XRD. The corresponding XRD patterns are shown in Fig. 4. The samples with different contents of RGO exhibit similar crystal composition compared to the original $\text{SiO}_2@\text{TiO}_2$ nanocomposite. The diffraction peaks at 25.3°, 37.8°, 48.0°, 54.0°, 55.1°, 62.7°, 68.4°, 70.3°, and 75.0° can be assigned to the diffractions of the (101), (004), (200), (105), (211), (204), (116), (220), and (204) crystal planes, respectively (JCPDS No 21-1272). The diffraction peaks at 6.5°, 42.5°, 50.1°, and 60° are supposed to originate from the SiO_2 core material (JCPDS No. 46-1045). No typical diffraction peaks corresponding to RGO was found which can be attributed to the low content of RGO in the $\text{SiO}_2@\text{TiO}_2/\text{RGO}$ nanocomposites and their relative low diffraction intensity. Furthermore, it can be concluded that the incorporation of RGO does not change the crystalline phases of TiO_2 .

The photocatalytic performance of $\text{SiO}_2@\text{TiO}_2/\text{RGO}$ nanocomposites. The photocatalytic activity of $\text{SiO}_2@\text{TiO}_2/\text{RGO}$ nanocomposites was evaluated by the photo-decolorization of RhB under UV irradiation.

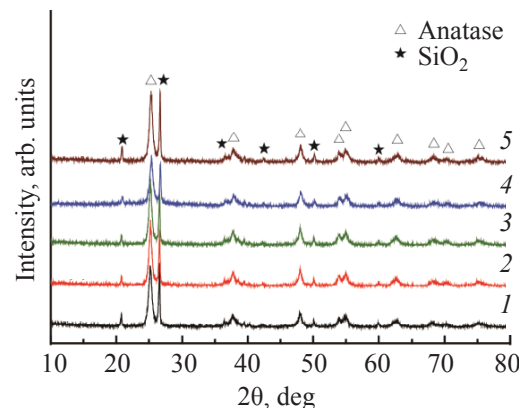


Fig. 4. XRD patterns of (1) $\text{SiO}_2@\text{TiO}_2$, (2) $\text{SiO}_2@\text{TiO}_2/\text{RGO}(1/0.005)$, (3) $\text{SiO}_2@\text{TiO}_2/\text{RGO}(1/0.05)$, (4) $\text{SiO}_2@\text{TiO}_2/\text{RGO}(1/0.1)$, and (5) $\text{SiO}_2@\text{TiO}_2/\text{RGO}(1/0.2)$.

Figure 5a and 5b shows the representative UV-vis spectra recorded during the photo-decolorization of RhB at the irradiation times of 0, 5, 10, 20, 40, and 60 min using $\text{SiO}_2@\text{TiO}_2$ and $\text{SiO}_2@\text{TiO}_2/\text{RGO}(1/0.05)$ as catalyst, respectively. It was worth to notice that when using $\text{SiO}_2@\text{TiO}_2/\text{RGO}(1/0.05)$ as catalyst (Fig. 5b), at the irradiation time of 0 min, the peak intensity of RhB at 554 nm was much lower than the initial peak intensity using $\text{SiO}_2@\text{TiO}_2$ as catalyst (Fig. 5a). That means the stronger adsorption ability for RhB of $\text{SiO}_2@\text{TiO}_2/\text{RGO}$ nanocomposites in comparison to pure $\text{SiO}_2@\text{TiO}_2$ catalyst. The pre-adsorbed capacity of RGO doped materials has been reported elsewhere. The effect of RGO doping on the adsorption ability of $\text{SiO}_2@\text{TiO}_2$ would be further explored afterward. By observing the UV-vis absorption spectra of RhB we can find that, with the increasing in irradiation time the peak intensity at 554 nm decreased without peak deviation, which suggests the bleaching of RhB.

Figure 6 shows the photodegradation rate of RhB over the catalysis of $\text{SiO}_2@\text{TiO}_2$ doping with different amount of RGO. Before reaction, the catalysts were firstly dispersed in RhB solution in dark for 30 min to get adsorption-desorption equilibrium. We could notice that, the samples showed different levels of adsorption capacity for RhB molecular. In the initial dark period, slight amount of RhB molecular were adsorbed onto $\text{SiO}_2@\text{TiO}_2$ and $\text{SiO}_2@\text{TiO}_2/\text{RGO}(1/0.005)$ surface. With the increase of RGO content, the adsorption capacity of the nanocomposites was highly improved. After 30 min, the ultraviolet light was switched on to perform the photodegradation reaction of RhB over several catalysts.

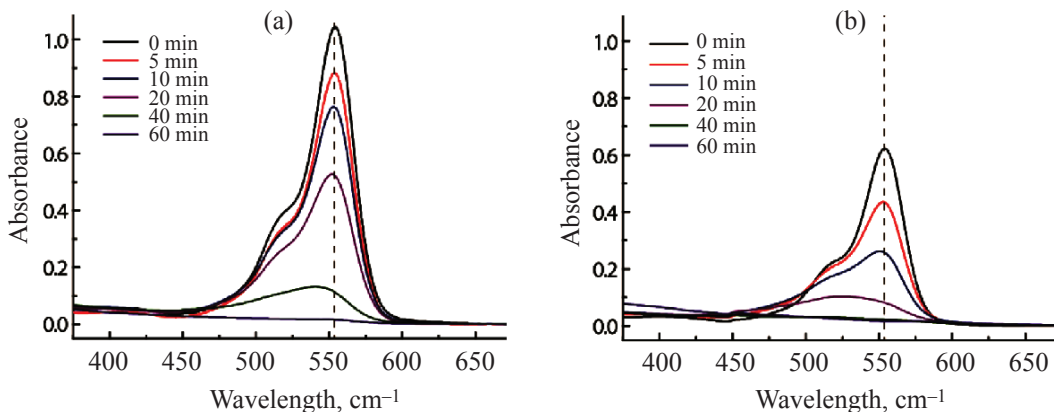


Fig. 5. Time-dependent UV-vis spectral changes of RhB catalyzed by (a) $\text{SiO}_2@\text{TiO}_2$ and (b) $\text{SiO}_2@\text{TiO}_2/\text{RGO}$ (1/0.05).

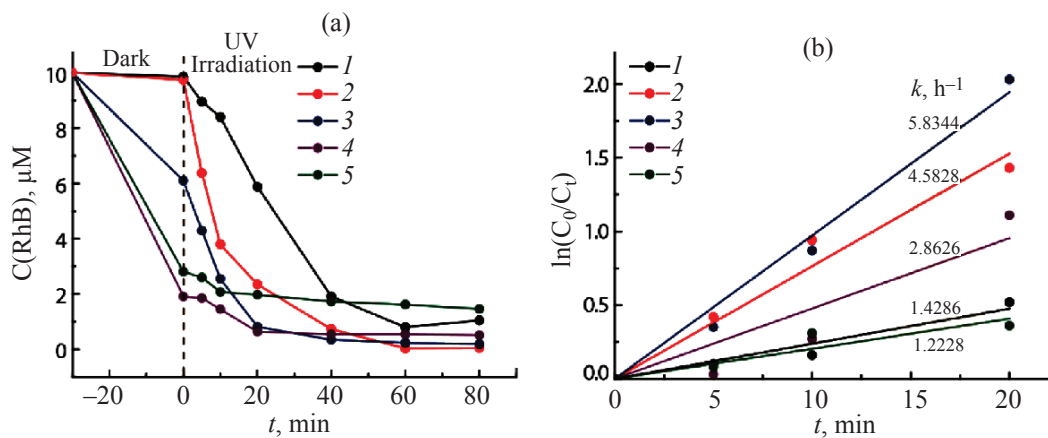


Fig. 6. (a) the degradation of RhB against the irradiation time over $\text{SiO}_2@\text{TiO}_2/\text{RGO}$ catalyst with different graphene doping (b) the kinetic plots for the RhB degradation, the according apparent rate constants were labeled, respectively. (1) $\text{SiO}_2@\text{TiO}_2$, (2) $\text{SiO}_2@\text{TiO}_2/\text{RGO}(1/0.005)$, (3) $\text{SiO}_2@\text{TiO}_2/\text{RGO}(1/0.05)$, (4) $\text{SiO}_2@\text{TiO}_2/\text{RGO}(1/0.1)$, and (5) $\text{SiO}_2@\text{TiO}_2/\text{RGO}(1/0.2)$.

It could be found that, even the pure $\text{SiO}_2@\text{TiO}_2$ catalyst showed much high degradation efficiency for RhB. Almost 90% of RhB could be decomposed after UV irradiation for 60 min over $\text{SiO}_2@\text{TiO}_2$ catalyst. The degradation efficiency was highly increased when RGO was doped onto $\text{SiO}_2@\text{TiO}_2$ with mass ratio of 1/0.005. When the mass ratio of RGO increased to 1/0.05, over 90% of RhB could be decomposed in 20 min. This is obvious that, the content of RGO plays an important role in improving the photocatalytic activity of $\text{SiO}_2@\text{TiO}_2$ nanocomposite. To clearly show the influence of RGO content on the photocatalytic efficiency of $\text{SiO}_2@\text{TiO}_2$ nanocomposite, the kinetic plots for the RhB photodegradation over series samples were shown in Fig. 6b. It could be clearly found that, the $\text{SiO}_2@\text{TiO}_2/\text{RGO}(1/0.005)$ sample showed the highest photocatalytic efficiency with an apparent rate constant of 5.9344, which was about 4 times greater than that of the pure $\text{SiO}_2@\text{TiO}_2$ (1.4286). The possible reason was that the

graphene could transfer the photo-excited electrons from TiO_2 particles quickly, thus effectively suppress the electron-hole recombination. The prolong lifetime of charge carriers in $\text{SiO}_2@\text{TiO}_2/\text{RGO}$ composites leads to more active oxidizing agents generation, which could improve the photo-degradation of RhB significantly in comparison to the $\text{SiO}_2@\text{TiO}_2$. More importantly, the enhanced adsorption kinetic may play a very important role in improving the photocatalytic degradation activity of $\text{SiO}_2@\text{TiO}_2/\text{RGO}$ photocatalyst due to the introduction of graphene. Interestingly, further increasing the mass ratio of RGO, the corresponding photocatalytic efficiency of $\text{SiO}_2@\text{TiO}_2/\text{RGO}$ was decreased to 2.8626 at mass ratio of 1/0.1 and 1.2228 at mass ratio of 1/0.2. This may probably be attributed to the increased scattering and absorbance of photons through excessive graphene in the photocatalytic system, which shields the light from reaching the surface of TiO_2 photocatalysts.

CONCLUSIONS

A series of core-shell structured $\text{SiO}_2@\text{TiO}_2/\text{RGO}$ composites have been prepared by versatile kinetics-controlled coating method and the RGO are deposited by UV-assisted photocatalytic reduction reaction. The corresponding photocatalytic performance has been investigated by photodegradation of RhB. We found that, the addition of RGO significantly enhanced the adsorption ability to RhB. As the increasing of RGO amount, the degradation rate of RhB was firstly increased and then decreased at excessive amount of RGO. The optimized ratio of $\text{SiO}_2@\text{TiO}_2$ to RGO was 1/0.05, at which the degradation efficiency of RhB was 4 times comparing with that of pure $\text{SiO}_2@\text{TiO}_2$ composite. The presence of RGO can both improve the adsorption capacity of RhB and enhance the fast separation of hotogenerated electron and hole pairs, thus promoting the degradation of organic dye.

ACKNOWLEDGMENTS

This work was financially supported by the Natural Science Foundation of Heilongjiang Province of China [QC2017005], the Cultivating Fund and Scientific Research of Northeast Petroleum University [grant no. 2017PYQZL-06]. We are also grateful for the measurement assistants from Analysis & Testing Center of Northeast Petroleum University.

REFERENCES

1. Belhadi, A., Boumaza, S., and Trari, M., *Appl. Energ.*, 2011, vol. 88, pp. 4490–4495.
2. Zhang, Y., Tang, Z. R., Fu, X., and Xu, Y. J., *Acs Nano*, 2011, vol. 5, pp. 7426–7435.
3. Albu, S. P., Ghicov, A., Aldabergenova, S., Drechsel, P., Leclerc, D., and Thompson, G.E., *Adv. Mater.*, 2010, vol. 20, pp. 4135–4139.
4. Wang, J. and Lin, Z., *J. Phys. Chem. C*, 2009, Vol. 113, pp. 4026–4030.
5. Xu, X., Feng, B., Zhou, G., Bao, Z., and Hu, J., *Mater. Design*, 2016, vol. 101, pp. 95–101.
6. Zhang, J., Kusumawati, Y., and Pauperté, T., *Electrochimica Acta*, 2016, vol. 201, pp. 125–133.
7. Hao, X., Jin, Z., Xu, J., Min, S., and Lu, G., *Superlattice. Microst.*, 2016, vol. 94, pp. 237–244.
8. Yu, Y.H., Chen, Y.P., and Cheng, Z., *Int. J. Hydrogen Energ.*, 2015, vol. 40, pp. 15994–16000.
9. Xu, T., Zhang, L., Cheng, H., and Zhu, Y., *Appl. Catal. B Environ.*, 2011, vol. 101, pp. 382–387.
10. Fan, W., Lai, Q., Zhang, Q., and Wang, Y., *J. Phys. Chem. C*, 2011, vol. 115, pp. 10694–10701.
11. Liu, F., Yan, X., Chen, X., Tian, L., Xia, Q., and Chen, X., *Catal. Today*, 2016, vol. 264, pp. 243–249.
12. Wang, H., Yuan, X., Zeng, G., Wu, Y., Liu, Y., and Jiang, Q., *Adv. Colloid Interface*, 2015, vol. 221, pp. 41–59.
13. Zielińska-Jurek, A., Kowalska, E., Sobczak, J.W., Lisowski, W., Ohtani, B., and Zaleska, A., *Appl. Catal. B Environ.*, 2011, vol. 101, pp. 504–514.
14. Du, J., Lai, X., Yang, N., Zhai, J., Kisailus, D., and Su, F., *Acs. Nano*, 2011, vol. 5, pp. 590–596.
15. Serpone, N., *J. Phys. Chem. B*, 2007, vol. 110, pp. 24287–24293.
16. Tingli, M., Morito, A., Eiichi, A., and Imai, I., *Nano Lett.*, 2005, vol. 5, pp. 2543–2547.
17. Manga, K.K., Wang, S., Jaiswal, M., Bao, Q., and Loh, K.P., *Adv. Mater.*, 2010, vol. 22, pp. 5219–5219.
18. Zhang, X.Y., Li, H.P., Cui, X.L., and Lin, Y., *J. Mater. Chem.*, 2010, vol. 20, pp. 2801–2806.
19. Zhou, F. and Zhu, Y., *J. Adv. Ceram.*, 2012, vol. 1, pp. 72–78.
20. Kim, S., Yin, Y., Alivisatos, A.P., Somorjai, G.A., and Jr, Y.J., *J. Am. Chem. Soc.*, 2007, vol. 129, pp. 9510–9513.
21. Crossland, E. J., Noel, N., Sivaram, V., Leijtens, T., Alexander-Webber, J.A., and Snaith, H.J., *Nature*, 2013, vol. 495, pp. 215–219.
22. Shekhah, O., Ranke, W., Schüle, A., Kolios, G., and Schlägl, R., *Angew. Chem. Int. Edition*, 2003, vol. 42, pp. 5760–5763.
23. Lee, H.W., Jin, Y.O., Lee, T.I., Jang, W.S., Yoo, Y. B., and Chae, S.S., *Appl. Phys. Lett.*, 2013, vol. 102, pp. 193903–193904.
24. Zhu, Y., Zhang, L., Yao, W., and Cao, L., *Appl. Surf. Sci.*, 2000, vol. 158, pp. 32–37.
25. Ji, L., Lin, Z., Alcoutlabi, M., and Zhang, X., *Energ. Environ. Sci.*, 2011, vol. 4, pp. 2682–2699.
26. Lee, J., Ji, C.P., and Song, H., *Adv. Mater.*, 2008, vol. 20, pp. 1523–1528.
27. Xiong, Z., Zhang, L.L., Ma, J., and Zhao, X.S., *Chem. Commun.*, 2010, vol. 46, pp. 6099–60101.
28. Li, K.T., Hsu, M.H., and Wang, I., *Catal. Commun.*, 2008, vol. 9, pp. 2257–2260.
29. Helden, A.K.V., Jansen, J.W., and Vrij, A., *J. Colloid Interf. Sci.*, 1981, vol. 81, pp. 354–368.
30. Ji, B. J., Qiao, Z., Lee, I., Dahl, M., Zaera, F., and Yin, Y., *Adv. Funct. Mater.*, 2012, vol. 22, pp. 166–174.
31. Zhang, H., Lv, X., Li, Y., Wang, Y., and Li, J., *Acs. Nano*, 2010, vol. 4, pp. 380–386.
32. Nethravathi, C. and Rajamathi, M., *Carbon*, 2008, vol. 46, pp. 1994–1998.